

# Computer-Aided Generation of Nonlinear Reduced-Order Dynamic Macromodels—II: Stress-Stiffened Case

Jan E. Mehner, Lynn D. Gabbay, and Stephen D. Senturia, *Fellow, IEEE*

**Abstract**—Reduced-order dynamic macromodels to describe the behavior of microelectromechanical system structures with stress stiffening are presented in this paper. The approach is based on potential and kinetic energy representations of selected fundamental modes of motion, modified to take account of stress stiffening. Energy data are calculated by several finite-element runs, fitted to polynomial functions, and used to develop the equations of motion according to Lagrangian mechanics. Accuracy and restrictions of these macromodels will be shown. [449]

**Index Terms**—Basis-function methods, CAD, electrostatic actuation, energy methods, macromodels, modal analysis, nonlinear vibrations, reduced-order models, stress stiffening.

## I. INTRODUCTION

IN PART ONE of this paper [1], a highly automated method for generating reduced-order dynamic macromodels for electrostatically actuated microelectromechanical system (MEMS) devices was presented. The approach was to use selected linear elastic modes of the device as basis functions, and to express the kinetic and potential energy in terms of basis-function amplitudes and their time derivatives. It was demonstrated that his procedure could indeed be executed nearly automatically, requiring only a few inputs from the designer to select parameters for the macromodel. However, while the procedure works well for nonlinearities produced outside the elastic body, such as the nonlinear *electrostatic* force between the plates of a parallel-plate capacitor with one plate being flexible, it fails to capture the correct *mechanical* structural stiffness when the deflections become comparable to a typical thickness [1, Fig. 12]. This effect is generally referred to as stress stiffening, and is a well-known effect in mechanics (see, e.g., [2]).

Manuscript received May 18, 1999; revised November 29, 1999. This work was supported by the Defense Advanced Research Projects Agency Microsystems Technology Office Microelectromechanical Systems Program under Contract J-FBI-95-215. Subject Editor, K. D. Wise.

J. E. Mehner was with the Microsystems Technology Laboratories, Massachusetts Institute of Technology, Cambridge, MA 02139 USA. He is now with the Chemnitz University of Technology, Chemnitz D-09107, Germany (e-mail: mehner@infotech.tu-chemnitz.de).

L. D. Gabbay was with the Microsystems Technology Laboratories, Massachusetts Institute of Technology, Cambridge, MA 02139 USA. He is now at 1301 Shoreway Road, Belmont, CA 94002 USA (e-mail: ldgabbay@alum.mit.edu).

S. D. Senturia is with the Microsystems Technology Laboratories, Massachusetts Institute of Technology, Cambridge, MA 02139 USA (e-mail: sds@mit.edu).

Publisher Item Identifier S 1057-7157(00)04861-7.

In simplest terms, stress stiffening results from the fact that when a clamped structure bends, it must get longer; therefore, it develops an axial stress. The elastic stored energy associated with this axial stress adds to the overall structural stiffness. In design, this nonlinearity should either be minimized for linear sensor and actuator applications or can be used on purpose to tune the stiffness or resonance frequencies for special problems [3], [4].

In this paper, we show that while the linear normal modes do not provide an adequate basis set with which to compute elastic stored energy in stress-stiffened cases, it is nevertheless possible to construct extremely accurate nonlinear stress-stiffened macromodels with basis functions that are very close to the linear normal modes. The failure of the linear normal modes was already demonstrated in [1, Fig. 12], but some additional discussion of the detailed reason for this failure is required here to motivate the particular approach we have taken. Furthermore, some background on the types of effects to expect in the presence of mechanical nonlinearities is useful.

The following section provides the theoretical background, leading to a discussion in Section III of the approach we have taken toward macromodeling of stress-stiffened devices. Dynamic results of macromodel simulations are compared with explicit nonlinear finite-element model (FEM) simulations in Section IV.

## II. THEORETICAL BACKGROUND

### A. Modal Methods for Nonlinear Systems

The use of modal methods for linear structural analysis has a long history (see, e.g., [5]). Finding efficient ways of using modal methods for nonlinear systems is still a research subject. A useful starting point is the review article of Rosenberg [6]. Investigations have focused on discrete elements, such as beams and plates, to explore the harmonic response. Of particular interest are the effects of nonlinearities on system behavior such as resonances, instabilities, and jump phenomena.

Recent contributions can be divided into two different approaches [7]. The first group assumes a harmonic time function and determines the spatial deflection of a structure. Therefore, one can use the method of harmonic balance [7]–[9] to obtain a nonlinear boundary-value problem and solve this by the FEM. This technique is preferred to compute the mode shape of nonlinear systems at resonance and the corresponding free-oscillation frequencies [10], [11].

In the second group, which includes [1], the motion  $u(r, t)$  is expanded in a series of spatial basis functions  $\varphi_i(r)$

$$u(r, t) = u_{\text{eq}}(r) + \sum_{i=1}^m q_i(t) \varphi_i(r) \quad (1)$$

where  $\varphi_i$  are the basis functions,  $q_i$  are the generalized coordinates,  $r$  is the spatial vector,  $t$  is the time of the system, and where, in keeping with the notation of [1],  $u_{\text{eq}}(r)$  is the static equilibrium position of the structure, providing for possible relaxation of initial stresses upon release of the microstructure. When the mechanical behavior is completely linear, it is useful to use the linear modes of vibration for the  $\varphi_i$ , as was done in [1]. However, even when the problem is mechanically nonlinear, the linear normal modes can serve as basis functions. The approach can be outlined as follows [7].

- 1) Compute the linear modes  $\varphi_i$  of the elastic problem.
- 2) Substitute  $u(r, t)$  in the governing equation for the deflection (e.g., the Euler–Bernoulli equation for beams).
- 3) Obtain a system of  $m$ -coupled second-order ordinary differential equations for the  $q_i(t)$ .
- 4) Solve the equations by perturbation techniques [9] to compute the dynamic response.

Both techniques have been successfully applied in modal dynamics. The second method, dealing with a series of linear mode shapes, is preferred for simulating the transient response to applied external loads and is, therefore, used in this paper in a modified way.

Most of the existing studies deal with vibrations close to resonance [12], [13]. It has been proven that mode shapes with invariant properties for nonlinear systems exist [6]. These deflection-dependent mode shapes are known as nonlinear normal modes (NNM's) and are surveyed in [7]. Modes are invariant if the motion is comprised in that mode at all times and does not generate any motion in the other modes. On the other hand, stimulated motions of one of the linear modes would exchange energy to other linear modes due to nonlinear mode coupling. Nevertheless, this energy exchange can be captured by the coupling terms that are obtained in 3) of the above procedure.

The approach we will take is to use a basis function expansion. The primary benefit of this approach is that it can be formulated independent of the details of the applied external forces and, thus, is well suited for MEMS actuators.

### B. Effects of Mechanical Nonlinearities

Many continuous systems, such as straight fixed-fixed beams with clamped ends, have cubic nonlinearities arising from mid-plane stretching. The dynamics of the fundamental mode of such structures are described by the Duffing equation [7]

$$\ddot{u} + 2\xi\omega_0\dot{u} + \omega_0^2 u + \varepsilon u^3 = F \cos(\Omega t) \quad (2)$$

where  $u$  is the generalized deflection,  $\xi$  is the modal damping ratio,  $\omega_0$  is the natural frequency associated with the linear system,  $\varepsilon$  determines the nonlinearity, and  $F \cos(\Omega t)$  is an externally applied generalized force.

In the following, we want to consider weakly nonlinear systems ( $\varepsilon \ll 1$ ) at harmonic excitation. One important feature is resonance. According to the linear theory, resonance occurs

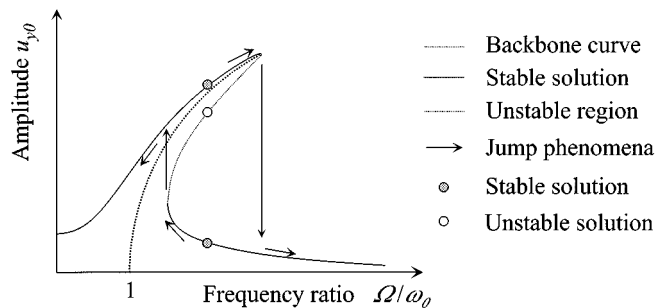


Fig. 1. Illustrating the frequency response for the Duffing equation with positive  $\varepsilon$  (stress stiffened).

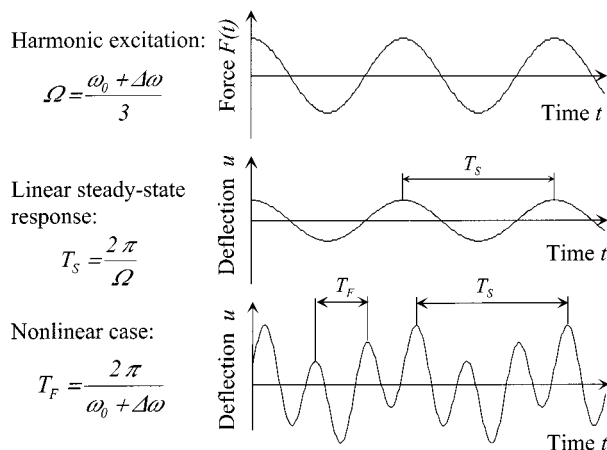


Fig. 2. Steady-state response for  $\Omega = (\omega_0 + \Delta\omega)/3$ , with  $\Delta\omega$  small.

when the driving frequency  $\Omega$  is close to the natural frequency  $\omega_0$ . This case is called primary or main resonance. The amplitude in response to any harmonic excitation is determined by the usual peaked resonance curve. However, for a system with a Duffing nonlinearity, the frequency response is like that of Fig. 1. Compared to the linear case ( $\varepsilon = 0$ ), a hardening nonlinearity ( $\varepsilon > 0$ ) bends the curve to the right-hand side (stress stiffening) and a softening nonlinearity ( $\varepsilon < 0$ ) would bend the curve to the left-hand side. This bending of the frequency response curve leads to multiple equilibrium states at some frequencies and, hence, to jump phenomena. The state depends on the initial conditions and the time dependence of the driving function. Jumps in amplitudes occur if the system changes its equilibrium state from one position to another one at the same frequency.

Another attribute of nonlinear systems is the secondary resonance. Those further resonances occur if the free-oscillation frequency is changed by the nonlinearity to exactly one-third or three times the frequency of the excitation (the factor three is due to the cubic nonlinearity). The first one is called subharmonic and the second one is called superharmonic resonance.

The transient response at subharmonic excitation is shown in Fig. 2. Even in the presence of damping, which in a linear system causes the natural response at frequency  $\omega_0$  to die out, in the nonlinear system, the response at the resonance frequency is actually driven and, hence, persists. The linear steady-state response contains only the forced response, while the nonlinear steady-state response includes both the forced response at the

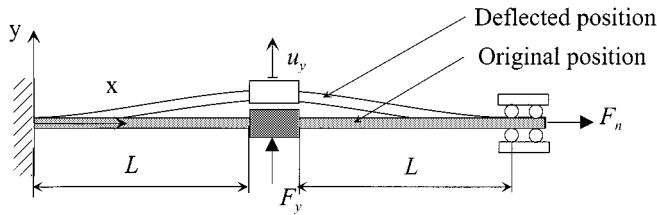


Fig. 3. Flexible beams supporting a rigid shuttle (subjected to axial and transverse forces).

drive frequency and the third harmonic of the drive, which is near to its resonance. Other nonlinear effects associated with multiharmonic excitations are discussed in [7].

The accuracy of the modal dynamic can be improved if more than one mode is taken into account. This is especially necessary in the case of fixed-fixed beams when the curvature near the clamps is high for large deflection amplitudes [15].

### C. Stress Stiffening Examples

Stress stiffening has the effect of coupling the in-plane and transverse displacements of beams and plates [14]. It is particularly important in thin structures, such as microstructures, where the bending stiffness is small compared to the axial stiffness. Fig. 3 illustrates a simple example of this effect.

The arrangement in Fig. 3 shows a typical microsystem configuration. A transverse force  $F_y$  leads to a deflection  $u_y$  of the shuttle. As soon as an axial force  $F_n$  acts on the beam, we see nonlinear behavior. For moderate axial loads compared to the buckling load, the stiffness  $K$  of the beam is nearly a linear function with respect to the axial force

$$K(F_n) = \frac{F_y}{u_y} \approx \frac{K_{\text{lin}}}{F_b} F_n + K_{\text{lin}} \quad (3)$$

where  $K_{\text{lin}}$  is the linear stiffness and  $F_b$  is the buckling force of the beam.

Axial forces can be caused not only by external loads, but also by internal stress  $\sigma$  or the deflection  $u_y$  itself. For a beam with clamped ends, we obtain

$$F_n \approx \sigma A + \frac{3EAu_y^2}{5L^2} \quad (4)$$

where  $E$  is Young's modulus and  $A$  is the cross section of the beam.

Equations (3) and (4) allow us to describe many systems that have straight fixed-fixed beams. Using other beam shapes like a folded beam design (see Fig. 4) can significantly reduce the stress-stiffening behavior, but it is still significant. In the general case, one has to solve the following Euler-Bernoulli equations:

$$EI \frac{\partial^4 u_y}{\partial x^4} - F_n(u_y) \frac{\partial^2 u_y}{\partial x^2} = f_y(x) \quad (5)$$

$$F_n(u_y) = \frac{EA}{L} \left( \int_0^L \sqrt{1 + (u_y')^2} ds - L \right) \quad (6)$$

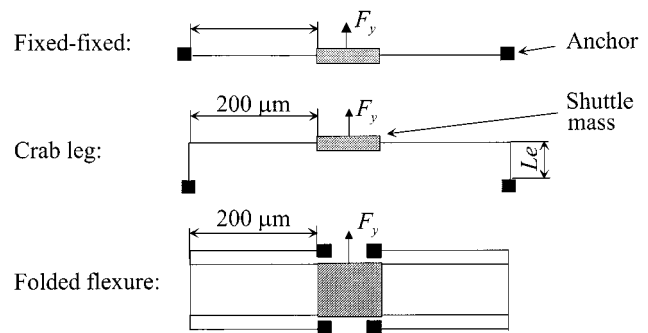


Fig. 4. Different arrangements to realize a linear motion.

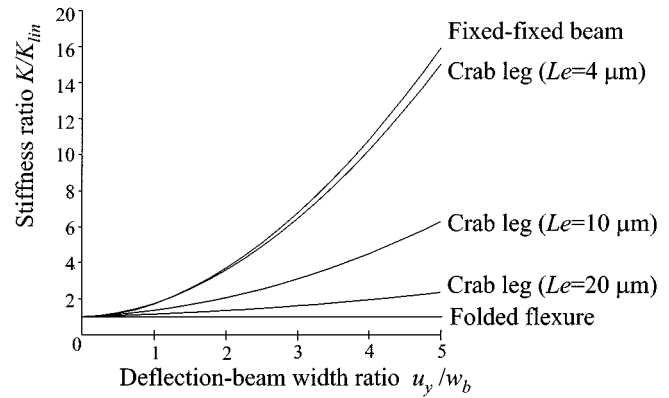


Fig. 5. Stiffness-deflection functions calculated with ANSYS.

where  $I$  is the moment of inertia and  $f_y$  is the transverse force per unit length. Equations (5) and (6) are usually applied with numerical techniques like the FEM or with perturbation techniques. Fig. 4 shows three typical spring designs used for many microstructures [3], [4].

Nonlinear stress stiffening occurs when the gradient with respect to displacement of the strain energy due to stretching of the neutral surface becomes comparable to the gradient of the strain energy due to bending. For fixed-fixed beams, this occurs when the deflection becomes comparable to the beam thickness. For this class of microstructures, the stiffness ratio function  $K/K_{\text{lin}}$  is nearly independent of the beam length, thickness, and Young's modulus. Essentially, the linear deflection range of crab legs can be increased by a longer leg length  $Le$ . However, long legs decrease the in-plane rotational stiffness. A folded flexure is used in many MEMS devices because of its excellent linearity in a large deflection range [4]. These spring arrangements show that a design of linear micromechanical systems is possible, but hard to realize (see Fig. 5).

On the other hand, many systems are designed to be nonlinear. Most resonant sensors make use of the stress stiffening effect as a transducer principle. Examples are sensors where an external load (acceleration, pressure) deflects beams or plates and thereby instantly changes their stiffness and resonant frequency. This shift of the resonant frequency is then picked up capacitively.

Another important application of stress stiffening is the alteration of spring constants or oscillation frequencies during

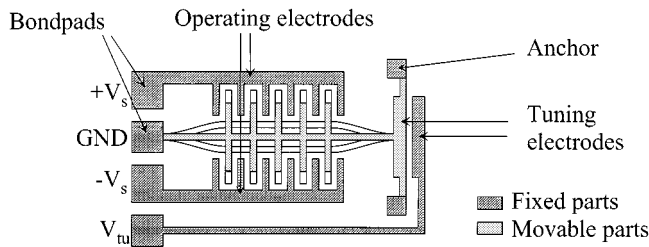


Fig. 6. Vibration sensor with frequency tuning based on stress stiffening [15].

the operation. This method can be used either to calibrate microstructures after the manufacturing process or to shift the stiffness for special applications such as vibration sensors [15].

The lateral stiffness and, hence, the vibration frequency of the element in Fig. 6, can be changed by the external voltage  $V_{tu}$ , in exact analogy to Fig. 3. Also, because the axial force  $F_n$  is controlled directly [see (3)], there is no amplitude dependence of the stiffness or resonant frequency, as normally results from electrostatic tuning methods [3].

### III. MACROMODEL CONSTRUCTION

#### A. General Approach

We now consider the application of the CHURN process presented in [1] to the problem of macromodel construction for stress-stiffened problems. The CHURN process begins with a vector of nodal displacements  $u$ . We will assume an electrostatically actuated elastic structure. The equations of motion, from [1], are of the form

$$[M] \frac{\partial^2 u}{\partial t^2} + F_m(u, t) - F_e(u, t) = 0 \quad (7)$$

where  $F_m$  is the nodally defined mechanical force, expressed as the gradient of the mechanical potential energy function  $U_m$

$$F_{m,i}(u, t) = \frac{\partial U_m(u, \dot{u}, t)}{\partial u_i} \quad (8)$$

and where  $F_e$  is the nodally defined electrostatic force, expressed as the gradient of the electrostatic potential coenergy function  $U_e^*$  (note the change of sign associated with the co-energy)

$$F_{e,i}(u, t) = \frac{\partial U_e^*(u, \dot{u}, t)}{\partial u_i}. \quad (9)$$

When the nodal displacements are represented as a superposition of linear normal modes  $\varphi_i(r)$ , as in (1), the equations of motion become

$$[M_G] \frac{\partial^2 q}{\partial t^2} + F_m(q, t) - F_e(q, t) = 0 \quad (10)$$

where  $M_G$  is the global mass matrix (it is diagonal),  $F_e(q, t)$  is the electrostatic actuation force, expressed in modal coordinates using the CHURN process of [1], and  $F_m(q)$  is a new quantity, the now *nonlinear* mechanical force, also expressed in modal coordinates.

It was demonstrated in [1, Fig. 12] that the direct application of the CHURN process to a mechanically nonlinear problem gives a large overestimate of the stiffness. The reason is that the

CHURN process displaces all nodes of the structure, which forbids Poisson contractions and the axial motions that typically accompany bending. Therefore, we decided to explore a modification of the CHURN process in which almost all degrees of freedom for the nodes are allowed to relax to the equilibrium position. This has the effect of restricting the class of problems we can solve, but within this restricted set, we find that the results are excellent.

We will start from a slightly modified form of the modal equations of motion. The dynamics of the  $i$ th modal amplitude can be written

$$M_i \ddot{q}_i + \frac{\partial U_m(q_1, \dots, q_i, \dots, q_N)}{\partial q_i} = \sum F \varphi_i + \int p \varphi_i dA \quad (11)$$

where instead of the explicit inclusion of electrostatic external forces, we now allow for both point loads ( $F$ ) and distributed loads ( $p$ ), whether mechanical or, in the case of distributed loads, electrostatic. The generalized mass  $M_i$  can either be calculated analytically from the mode shape

$$M_i = \int \rho \varphi_i dV \quad (12)$$

where  $\rho$  is the density of the structure, or it can be obtained from the result file of a finite-element modal analysis as the appropriate diagonal element of  $M_G$ , and where the integrals over the external forces project each force into modal coordinates.

#### B. Specific Approximations

We now restrict our attention to MEMS systems in which: 1) there is a dominant normal mode of motion; 2) there is a well-defined neutral surface for the structure; and 3) the largest motion in the structure is perpendicular to this neutral surface. While this appears to be a severe restriction, many electrostatically actuated MEMS devices obey these restrictions.

The specific modification to the CHURN process is that instead of imposing displacements on all degrees of freedom of all nodes, a modal displacement is represented as a *perpendicular displacement of the nodes of the neutral surface in the dominant direction*; nodes not on the neutral surface are not constrained. In addition, degrees of freedom orthogonal to the dominant displacement are not constrained for nodes in the neutral surface. With these restricted nodal displacements as a boundary condition, the elastic stored energy  $U_m$  is then computed using finite-element simulation, in exactly analogous fashion to the computation of  $U_e^*$ .

There are three important effects of this removal of nodal constraints when making a modal displacement. First, Poisson contractions are allowed. Second, nodal displacements perpendicular to the dominant direction are now allowed for nodes originally in the neutral surface. These two effects mean that the extraneous strain energy of the original CHURN process is largely avoided and, as will be shown below, the resulting elastic energy is very close to the correct equilibrium value. The third effect is more subtle. By allowing these various nodal relaxations, the resulting final shape is no longer the same as the original normal mode  $\varphi_i(r)$ . The relaxed function, which we shall call  $\eta_i(r)$ , differs from  $\varphi_i(r)$  by a small, but not unimportant amount. It

is precisely this difference that allows the strain energy to be correct for the equivalent modal displacement in the dominant direction. Furthermore, we use the gradients of  $U_m$  calculated with these modified basis functions as the mechanical force in the original equations of motion. In effect, we are saying that by allowing extremely small changes to the basis functions, we obtain a strain energy function whose gradient is a good approximation to the elastic forces when expressed in  $q$ -space.

In addition to these important assumptions about nodal constraints and strain-energy gradients, we use a perturbation approximation to calculate the strain energy, as explained in the following section.

### C. Computing the Strain Energy Function

Since we have restricted our attention to structures with a dominant mode of deformation, we could imagine calculating the elastic strain energy as a series of decreasing terms

$$\begin{aligned} U_m(q_1, \dots, q_m) &= U_m(q_1, q_2, 0, \dots, 0) \\ &+ [U_m(q_1, q_2, q_3, \dots, 0) - U_m(q_1, q_2, 0, \dots, 0)] \\ &+ \dots + [U_m(q_1, q_2, q_3, \dots, q_m) \\ &- U_m(q_1, q_2, \dots, q_{m-1}, 0)] \end{aligned} \quad (13)$$

where, assuming the modes are taken up in order of their importance, each square bracketed term is smaller than all terms that precede it. We make one further approximation in this type of series. We denote

$$W_{12} = U_m(q_1, q_2, 0, \dots, 0) \quad (14)$$

and for  $j > 2$ ,  $W_{1j}$  as the corresponding square bracketed term above

$$\begin{aligned} W_{1j} &= U_m(q_1, q_2, \dots, q_{j-1}, q_j, \dots, 0) \\ &- U_m(q_1, q_2, \dots, q_{j-1}, 0, \dots, 0) \end{aligned} \quad (15)$$

and we specifically approximate  $W_{1j}$  as

$$W_{1j} \cong U_m(q_1, 0, \dots, 0, q_j, \dots, 0) - U_m(q_1, 0, \dots, 0). \quad (16)$$

That is, when computing the strain energy contribution of the higher order modes, we consider various combinations of mode 1 with that higher order mode, but with all other higher order mode amplitudes set to zero. This approximation has been shown to yield insignificant errors, while greatly reducing the number of FEM runs needed to span the  $q$ -space for the selected modes of interest.

Typically, the strain energy for structures with stress stiffening can be expressed as a fourth-order polynomial in the modal amplitudes. For a structure with five important modes, it requires about 100 FEM simulations to compute the strain energy. This strain energy is then fitted to a fourth-order polynomial in the modal amplitudes, and appropriate gradients are taken and inserted into the dynamic equations of motion.

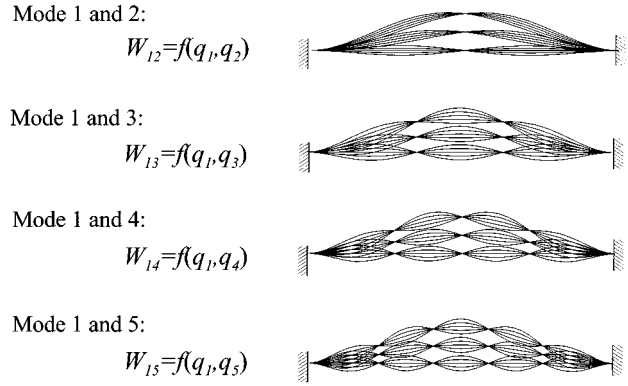


Fig. 7. Sets of displacements for calculating the strain energy of a clamped beam.

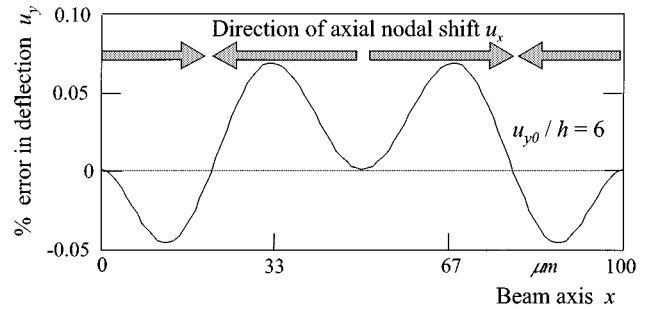


Fig. 8. Deflection error of mode shape 1 due to the node shift in axial direction for a displacement of six times the beam thickness.

### D. Example: Clamped Beam

Fig. 7 illustrates the various combinations of mode 1 and higher order modes of a clamped beam used to compute the various contributions to the strain energy.

As stated earlier, since we allow nodes originally in the neutral surface to displace perpendicular to the dominant direction of motion, the modal functions  $\eta_i(r)$  differ from the original  $\varphi_i(r)$  even at the neutral surface, but the error that results in displacement in the dominant direction is quite small. The error is a function of the slope (first derivative of  $u_y$  in the axial direction) and was calculated analytically for a clamped beam (Fig. 8). Since the slope is, in general, small for structures with stress stiffening, this effect can be neglected for most problems.

With this assumption in mind, we can assess the accuracy of the strain energy calculations based in the FEM against the exact analytical solution for straight beams

$$U_m = \frac{EI}{2} \int_0^L (u'')^2 ds + \frac{EA}{2L} \left( \int_0^L \sqrt{1 + (u')^2} ds - L \right)^2 \quad (17)$$

where  $u'_y$  is the first and  $u''_y$  is the second derivative of the bending line and  $L$  is the beam length.

The relative strain energy error depends somewhat on the discretization, but is always below 0.5% for a reasonable meshed structure (Fig. 9).

A very important feature of nonlinear mechanical systems is that the strain energy functions may be asymmetric. Fig. 10 illustrates that the energy minimum (dashed line) leaves the zero

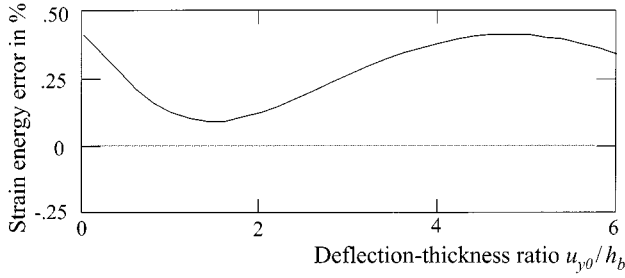


Fig. 9. Strain energy error as a function of the deflection amplitude.

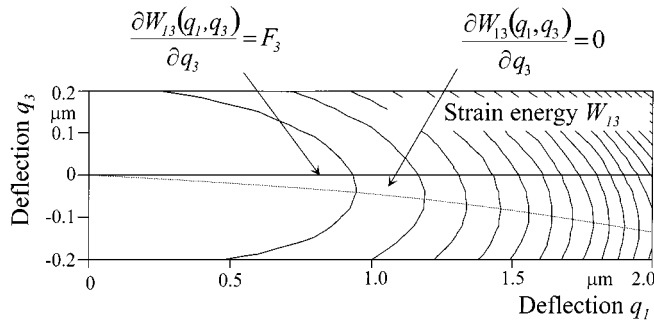
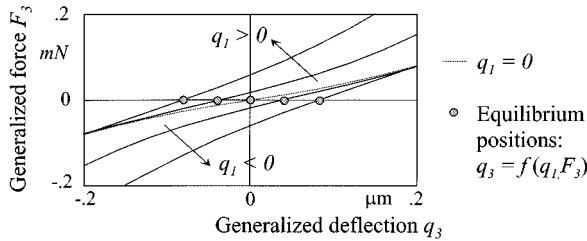
Fig. 10. Contour plot of the asymmetric strain energy function  $W_{13} = f(q_1, q_3)$  for a fixed-fixed beam.

Fig. 11. Force-deflection function and equilibrium positions of mode 3 with respect to mode 1.

deflection line of mode 3 (solid line) as soon as mode 1 is growing ( $F_3 = 0$ ). This attribute has to be accurately captured by the macromodel because it describes all interactions between the modes, which are essential for the modal dynamics.

Calculating the modal force functions, which are the derivatives of the strain energy with respect to the generalized coordinate (at that deflection), we recognize that the curve does not necessarily strike the origin (Fig. 11). That means as soon as mode 1 is deflected, we get a force acting on other modes. If there is enough time (quasi-static systems) and there are no external forces, higher modes follow exactly the dashed line in Fig. 10. As a consequence, the bending line of fixed-fixed beams gets flatter with growing amplitudes (Fig. 12), as is observed in numerous measurements [13].

After the set of finite-element simulations is completed, the nonlinear function fitting is done by the Levenberg–Marquardt method [16]. This well-known method is implemented in MathCad [17], but is also available in public-domain software

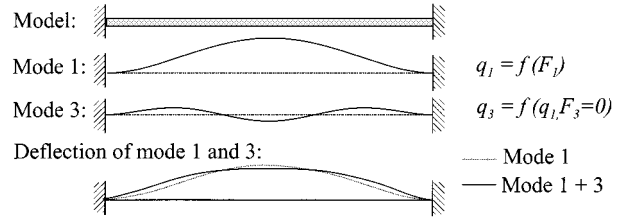


Fig. 12. Typical shape change near the clamps of beams at large deflection amplitudes.

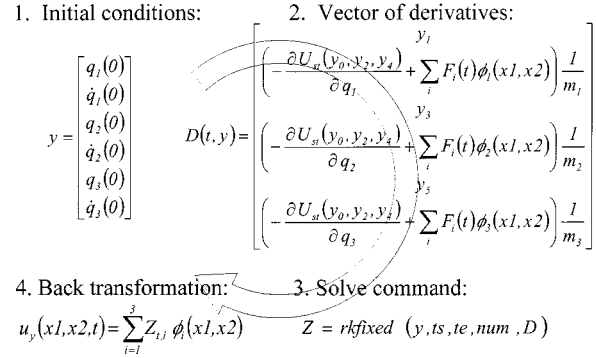


Fig. 13. MathCad notation to solve the equations of motion.

tools. The function fitting has to be applied to the strain energy functions according to (16) and all mode shapes. In case of systems where a nearly rigid plate is supported by beams, the mode shapes should be fitted for each beam separately.

### E. Solving the Equations of Motion

Finally, the system is described by a nonlinear system of ordinary differential equations, which are solved numerically by the Runge–Kutta scheme. An automated time-stepping algorithm is recommended for problems with varying dynamics. Notice that in case of stiff equations (i.e., where the matrix gets nearly singular), the numerical solution may oscillate or be unstable. In this frequently occurring case, one could replace the Runge–Kutta with the Bulirsch–Stoer or Rosenbrock methods [18]. The required syntax for a system with three relevant modes is depicted in Fig. 13.

## IV. RESULTS AND DISCUSSION

### A. Quasi-Static Deflections

The accuracy, robustness, and convergence behavior of this modeling approach will be demonstrated in this section through a set of examples. The first example is an electrostatically actuated fixed-fixed beam suspended above an electrode strip. The dimensions and material properties are the same as given in [1, Fig. 8]. As was done in [1], we can use the dynamical modal equations in dc steady state to calculate the static displacement, and compare it to the full self-consistent three-dimensional (3-D) simulation with CoSolve-EM [19], which is a

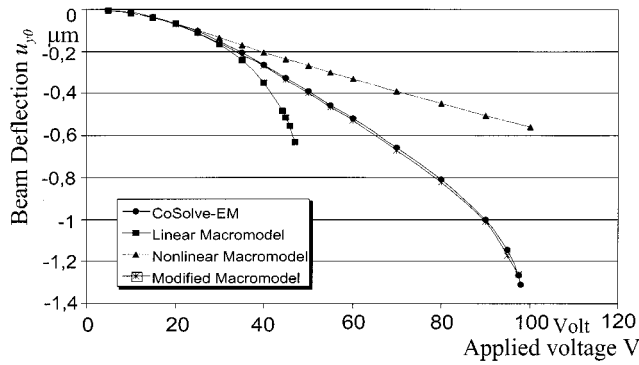


Fig. 14. Voltage-deflection function for a fixed-fixed beam.

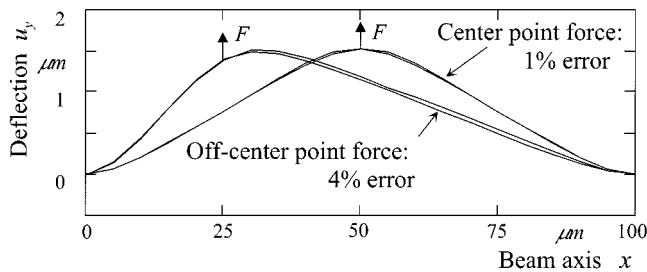


Fig. 15. Deflection calculated by the macromodel and FEM.

part of the MEMCAD system.<sup>1</sup> For the modal solution, the electrostatic force is calculated analytically, neglecting the fringing field (the beamwidth  $w_b$  is much larger than gap separation  $d$ ). Equilibrium occurs if the derivatives of the strain energy function are equal to the derivatives of the electrostatic co-energy  $U_e^*$

$$U_e^* = \frac{V^2}{2} \int_0^L \frac{\epsilon_0 w_b}{d - \sum_{i=1}^m q_i \varphi_i} ds \quad (18)$$

where  $V$  is applied voltage and  $\epsilon_0$  is the permittivity of air.

The comparison is shown in Fig 14. In sharp contrast with [1, Fig. 12], we now see that the nonlinear macromodel agrees nearly perfectly with the CoSolve-EM solution. The difference between the nonlinear macromodel and the CoSolve-EM solution is about 2% over the entire voltage range. This shows that the various approximations concerning nodal degrees of freedom and strain-energy calculations give very good results.

In the next example, a single point-load force acts on the same beam instead of a distributed electrostatic load. In this case, the influence of higher modes get stronger and the accuracy of their interactions can be assessed. The first five modes are taken into account and antisymmetric modes are neglected. The structure is deflected far into the nonlinear range to positions about three times the beam thickness. That means the stiffness increases about 560% (Fig. 5). First, only mode 1, then modes 1 and 3, and finally, modes 1, 3, and 5 were modeled. We obtain a deflection error at the center of 5.6%, 3.9%, and 1.0%, respectively. Results are compared against a nonlinear 3-D finite-element analysis (Fig. 15).

Point loads are then applied at different position between the support and center. Antisymmetric modes are now included.

<sup>1</sup>Microcosm Technologies, Cambridge, MA. <http://www.memcad.com>

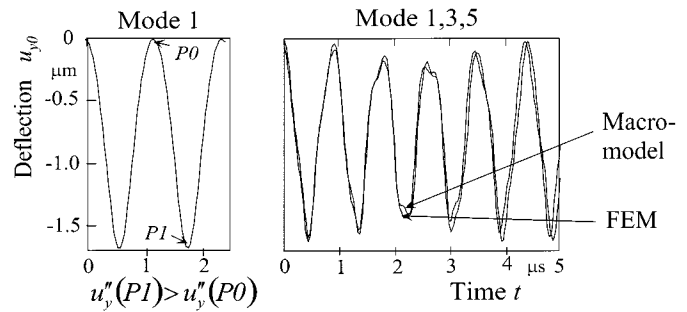


Fig. 16. Dynamic response to a suddenly applied force at the center of a beam.

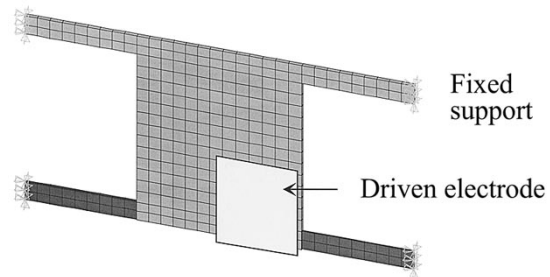


Fig. 17. Finite-element model of a plate with asymmetric support.

As long as the distance between the point of force application and the support is more than 25% of the beam length, mode 1 can still be considered as dominant. The deflection error along the beam axis increased slightly, but was always below 4% (Fig. 15).

### B. Undamped Transients

Now the transient behavior (without damping) is analyzed for the same clamped-beam model. The structure is driven by a suddenly applied point-load force at its center, and its deflection is calculated as a function of time.

As known from nonlinear systems, the deflection is, in general, a nonsinusoidal function. Mode 1 is most strongly distorted (Fig. 16). Both marked elongations  $P0$  and  $P1$  have a different curvature due to the deflection-dependent stiffness (curvature at  $P1$  is much bigger than at  $P0$ ). Applying the Fourier decomposition method, we observe higher harmonics of mode 1 in the response spectrum. Those frequencies may lie very close to the higher order modes of our structure and excite them strongly (internal resonance). As a result of these interactions, beat frequencies appear, especially if the structure is driven in the range of stress stiffening.

The last example proves the accuracy for a plate with an asymmetric support (Fig. 17). The same dimensions and material properties are taken as in [1, Fig. 3]. The three lowest modes of the structure are included in the macromodel. Two of these modes are primarily rotational. However, even in case of rotational degrees of freedom, the displacements of all finite-element nodes can be expressed by a translation (one dominant direction) as long as the rotations are small. Fig. 18 shows that the first three modes capture the transient behavior very well. Macromodels are, in general, a little less accurate than appropriate finite-element solutions. This deviation is mainly caused

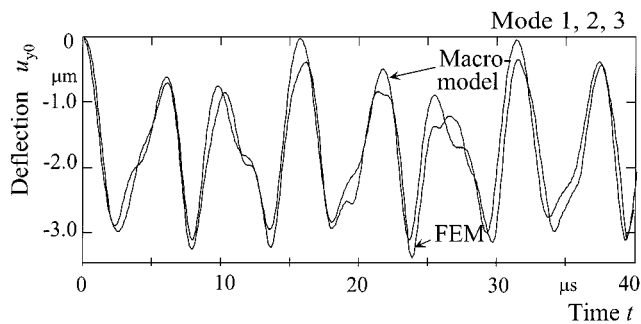


Fig. 18. Response of Fig. 17 structure to a voltage jump.

by the limited number of modes, and not errors in the strain energy extraction. The achieved accuracy is sufficient for many problems, especially if one considers the computational costs.

The time needed to establish a macromodel for structures with stress stiffening is primarily defined by the finite-element calculations. Considering five relevant modes, one needs about 100 quasi-static simulations. This is about the same time we would estimate is required to simulate the transient behavior of a microstructure during the first four oscillation periods. However, a macromodel once established can be used for many different load situations. We can include nonmechanical parts as well as systems with energy dissipation.

The procedure presented here has not yet been automated to the extent of the CHURN process in [1]. However, there does not appear to be any fundamental reason why it cannot be done. The designer must make more choices, such as identifying the dominant mode and specifying the dominant direction of displacement, and while our experience with the examples is very good, it is quite difficult to establish robust error bounds for the various assumptions and approximations used in this paper. That is a subject for further study.

## V. CONCLUSION

An important benefit of the macromodeling approach presented here is the extension of computationally efficient methods for generating nonlinear macromodels to systems with stress stiffening. Stress stiffening is relevant in many microstructures and is induced by the axial stress of structures restrained at the ends. When such a structure has a dominant deformation mode, it is now possible to construct accurate dynamical models based on linear mode shapes. The macromodel can then be used for any different load situation either for steady-state or dynamic simulations.

## ACKNOWLEDGMENT

The authors wish to thank Microcosm Technologies, Cambridge, MA, for extensive cooperation in interfacing MEMCAD 3.2 with the macromodeling tools developed here.

## REFERENCES

- [1] L. D. Gabbay, J. E. Mehner, and S. D. Senturia, "Computer-aided generation of reduced-order dynamic macromodels—I: Geometrically linear motion," *J. Microelectromech. Syst.*, vol. 9, pp. 262–269, June 2000.
- [2] J. S. Przemieniecki, *Theory of Matrix Structural Analysis*. New York: McGraw-Hill, 1968.

- [3] C. S. Lee, S. Han, and N. C. MacDonald, "Multiple depth, single crystal silicon microactuators for large displacements fabricated by deep reactive ion etching," in *Solid-State Sens. Actuator Workshop*, Hilton Head Island, SC, 1998, pp. 45–50.
- [4] L. Ristic, *Sensor Technology and Devices*. Norwood, MA: Artech House, 1994.
- [5] L. Meirovitch, *Analytical Methods in Vibrations*. New York: Macmillan, 1967.
- [6] R. M. Rosenberg, "On nonlinear vibrations of systems with many degrees of freedom," *Advances Appl. Mechanics*, vol. 9, pp. 155–242, 1966.
- [7] A. H. Nayfeh and D. T. Mook, *Nonlinear Oscillations*. New York: Wiley, 1979.
- [8] A. H. Nayfeh and S. A. Nayfeh, "On nonlinear modes of continuous systems," *J. Vibration Acoust.*, vol. 116, pp. 129–139, 1994.
- [9] A. H. Nayfeh, *Perturbation Methods*. New York: Wiley, 1973.
- [10] A. F. Vakakis, L. I. Manevitch, Y. V. Mekhlin, V. N. Pilipchuk, and A. A. Zevin, *Normal Modes and Localization in Nonlinear Systems*. New York: Wiley, 1996.
- [11] S. W. Shaw and C. Pierre, "Normal modes for nonlinear vibratory systems," *J. Sound Vibration*, vol. 164, pp. 85–124, 1993.
- [12] W. Szemplinska-Stupnicka, "Non-linear normal modes and the generalized ritz method in the problems of vibrations of nonlinear elastic continuous systems," *Int. J. Nonlinear Mechanics*, vol. 18, pp. 149–165, 1983.
- [13] R. Benamar, M. M. K. Bennouna, and R. G. White, "The effect of large vibration amplitudes on the mode shapes and natural frequencies of thin elastic structures part I: Simply supported and clamped-clamped beams," *J. Sound Vibration*, vol. 149, pp. 179–195, 1991.
- [14] S. Timoshenko and S. Woinowsky-Krieger, *Theory of Plates and Shells*. New York: McGraw-Hill, 1959.
- [15] T. Gessner and W. Doetzel, "Sonderforschungsbereich 379," in *Micromechanical Sensor and Actuator Arrays*. Chemnitz, Germany: Tech. Univ. Chemnitz, 1998.
- [16] *User's Guide to MINPACK I*, Argonne Nat. Lab., Argonne, France, 1980.
- [17] *Manual of MathCad 7.0 Professional*, MathSoft, Cambridge, MA, 1997.
- [18] J. Murphy, *Numerical Analysis Algorithms and Computation*. New York: Ellis Horwood Halsted Press, 1988.
- [19] J. R. Gilbert, R. Legtenberg, and S. D. Senturia, "3D coupled electromechanics for MEMS: Applications of CoSolve-EM," in *Proc. MEMS'95*, Amsterdam, The Netherlands, pp. 122–127.



**Jan E. Mehner** received the Diploma and the Dr.-Ing. degree in electrical engineering and information technology from the Chemnitz University of Technology, Chemnitz, Germany, in 1989 and 1994, respectively.

From 1998 to 1999 he was a Visiting Scientist at the Massachusetts Institute of Technology, Cambridge, where he was involved in the field of macromodeling. He is currently a Scientific Assistant in the Department of Microsystems and Precision Engineering, Chemnitz University of Technology. His research interests include analytical and numerical methods to design microsystems, computer-aided design (CAD) tools, and computational algorithms for problems with coupled fields.



**Lynn D. Gabbay** received the B.S. degree in applied physics and computer science from Cornell University, Ithaca, NY, in 1993, and the M.S. and Ph.D. degrees in electrical engineering and computer science from the Massachusetts Institute of Technology, Cambridge, in 1995 and 1998, respectively.

From 1994 to 1998, he performed research in the field of computer-aided macromodeling for MEMS. He is currently an Independent Consultant. His research interests include the design and implementation of automated macromodel construction algorithms, and the integration of these tools into existing system simulators.



**Stephen D. Senturia** (M'77–SM'91–F'93) received the B.A. degree in physics (*summa cum laude*) from Harvard University, Cambridge, MA, in 1961, and the Ph.D. degree in physics from the Massachusetts Institute of Technology, Cambridge, in 1966.

Since 1966, he has been with the Massachusetts Institute of Technology, where he is currently the Barton L. Weller Professor of Electrical Engineering. In 1982, he founded Micromet Instruments Inc., and served on its Board of Directors until 1992.

His current principal research activities are the development of CAD systems for design and simulation of MEMS devices and the use of microfabricated structures for both microsensor and microactuator applications, and for materials research.

Dr. Senturia is a member of Phi Beta Kappa and Sigma Xi. He is a trustee of the Transducer Research Foundation. He is a founding associate editor of the JOURNAL OF MICROELECTROMECHANICAL SYSTEMS (since 1992), and currently serves as a senior editor. He was the solid-state sensors associate editor of the IEEE TRANSACTIONS ON ELECTRON DEVICES (1985–1996) and has been an active participant in the organization and planning of major conferences on solid-state sensors and actuators since 1983. He is corecipient of an IR-100 Award for his work on automated reclamation of urban solid waste, and of the 1988 Arthur K. Doolittle Prize of the Division of Polymeric Materials Science and Engineering of the American Chemical Society.